Sources of Absorption and Scattering Contrast for Near-Infrared Optical Mammography[1]

Albert E. Cerussi, PhD, Andrew J. Berger, PhD,[2] Frederic Bevilacqua, PhD, Natasha Shah, BS, Dorota Jakubowski, MS
John Butler, MD, Randall F. Holcombe, MD, Bruce J. Tromberg, PhD

Rationale and Objectives. Near-infrared (NIR) diffuse optical spectroscopy and imaging may enhance existing technologies for breast cancer screening, diagnosis, and treatment. NIR techniques are based on sensitive, quantitative measurements of functional contrast between healthy and diseased tissue. In this study, the authors quantified the origins of this contrast in healthy breasts.

Materials and Methods. A seven-wavelength frequency-domain photon migration probe was used to perform noninvasive NIR measurements in the breasts of 28 healthy women, both pre- and postmenopausal, aged 18–64 years. A diffusive model of light transport quantified oxygenated and deoxygenated hemoglobin, water, and lipid by their absorption signatures. Changes in the measured light-scattering spectra were quantified by means of a "scatter power" parameter.

Results. Substantial quantitative differences were observed in both absorption and scattering spectra of breast as a function of subject age. These physiologic changes were consistent with long-term hormone-dependent transformations that occur in breast. Instrument response was not adversely affected by subject age or menopausal status.

Conclusion. These measurements provide new insight into endogenous optical absorption and scattering contrast mechanisms and have important implications for the development of optical mammography. NIR spectroscopy yields quantitative functional information that cannot be obtained with other noninvasive radiologic techniques.

Key Words. Breast, parenchymal pattern; breast radiography, technology; optical imaging.

This article describes the application of a new class of near-infrared (NIR) spectroscopy tools for noninvasive, quantitative characterization of breast tissue physiology.

Diagnostic methods currently in use, such as mammography, magnetic resonance imaging, and ultrasound (US), offer excellent anatomic lesion-detection capabilities but generally cannot provide quantitative information regarding tissue function and composition (1). Positron emission tomography shows great promise in evaluating the metabolic demands of tissue but requires exogenous radionuclides and is insensitive to tissue hemodynamics. NIR optical spectroscopy is intrinsically sensitive to the principal components of breast: blood, water, and adipose, as well as epithelial and connective tissues. Results of preliminary studies suggest that the fractional contribution of each component to NIR signals depends strongly on factors such as age, menopausal status, and the progression of disease. Thus, NIR optical spectroscopy provides an opportunity for revealing physiologic information that cannot otherwise be obtained noninvasively.

As optical diagnostic methods become more clinically applicable, there is a growing need to identify and quantify sources of endogenous contrast in breast (2–11). This article presents the results of quantitative NIR spectroscopic studies in 28 subjects ranging in age from 18 to 64 years. We provide evidence that NIR tissue spectroscopy is inherently sensitive to long-term age and hormone-dependent dynamics. Similar studies have been initiated (12–14) but in only a few subjects or with limited sensitivity to physiologic parameters. These data are expected to play an important role in characterizing the sensitivity of NIR optical spectroscopy and imaging for applications such as tumor detection, therapeutic monitoring, and risk assessment.

NIR photons (600–1,000 nm) are nonionizing and weakly absorbed by tissue. Many investigators have used them to explore brain, breast, and muscle tissue, exploiting their enhanced penetrance relative to that of visible or ultraviolet radiation (1). In breast tissue, the principal NIR absorbers are assumed to be reduced hemoglobin (Hb-R), oxygenated hemoglobin (Hb-O_2), water (H_2O), and lipids (15). NIR tissue spectroscopy offers a safe way to quantify these components and to view unique functional information with low-cost "point-of-care" devices. Multiple light scattering complicates quantitative measurements of light absorption in the NIR range. The process of using frequency-domain photon migration (FDPM) techniques to separate the effects of absorption from scattering has been described in detail (16,17). FDPM enables the use of quantitative spectroscopic analysis tools to determine the composition and structure of tissue noninvasively (18).

The application of FDPM techniques to NIR tissue spectroscopy differs substantially from conventional bulk NIR methods, such as diaphanography (19). FDPM employs computational models that allow the quantitative separation of the effects of absorption and scattering (20). Thus, within the limits of applicability of the light transport models to the breast, all parameters measured in this study are absolute values.

MATERIALS AND METHODS

Patient Selection

All volunteers enrolled in this study competently provided informed consent to participate in one of two trials (nos. 95-563 and 99-2183) under the guidelines of an Institutional Review Board. The 28 women ranged in age from 18 to 64 years. Fifteen of them were premenopausal (average age, 28 years ± 9), and seven were postmenopausal (average age, 56 years ± 2). The remaining six women (average age, 56 years ± 5) were taking some form of hormone replacement therapy (HRT); three of the six classified themselves as perimenopausal. None of the women had any known cancerous lesions or other known forms of breast disease.

Measurement Technique

Each subject rested in a supine position during the measurement. The instrument probe, slightly larger than a US probe (Fig 1), was the only item placed in contact with the subject. It consisted of a sealed APD module and an optical fiber placed 22 mm from the APD. All measurements were performed in a reflection-style geometry. The probe was placed on the breast with minimal pressure and only the force of gravity; no compression was used. In this configuration, we estimate that the mean sampling depth was approximately 1 cm below the skin. We report data only on measurements performed in the center of the left upper outer quadrant (measurements on the right upper quadrant yielded similar results). Error bars in the figures and tables represent the standard deviations (SDs) of repeated measurements.

Instruments

A schematic of our 1-GHz, portable FDPM device is shown in Figure 1. This FDPM instrument has been described in detail elsewhere (21). It employs multiple diode lasers that provide visible and NIR light at seven wavelengths (672, 800, 806, 852, 896, 913, and 978 nm). A hand-held probe has been designed to house an APD that records the modulated diffuse light signals after propagation through the tissue. This probe has a plastic attachment on the casing to position a source optical fiber a fixed distance from the APD. A 100-μm-diameter graded index optical fiber positioned 22 mm from the APD detector was used to deliver the diode laser outputs to the tissue surface. A network analyzer (8753c; Agilent, Palo Alto, Calif), measured the phase and amplitude of the detected electronic signal from the APD over a range of source modulation frequencies. A steady-state current source was mixed with radiofrequency power provided by the network analyzer in a bias network. This bias network serially distributed power to each laser diode and produced intensity-modulated light. An optical switch delivered light serially from each diode to the tissue via the single optical fiber described above. The optical power-launched into the tissue ranged from 5 to 25 mW for each wavelength.

A sweep over all seven wavelengths took approximately 35–60 seconds. The system acquired data in less than 3 sec-
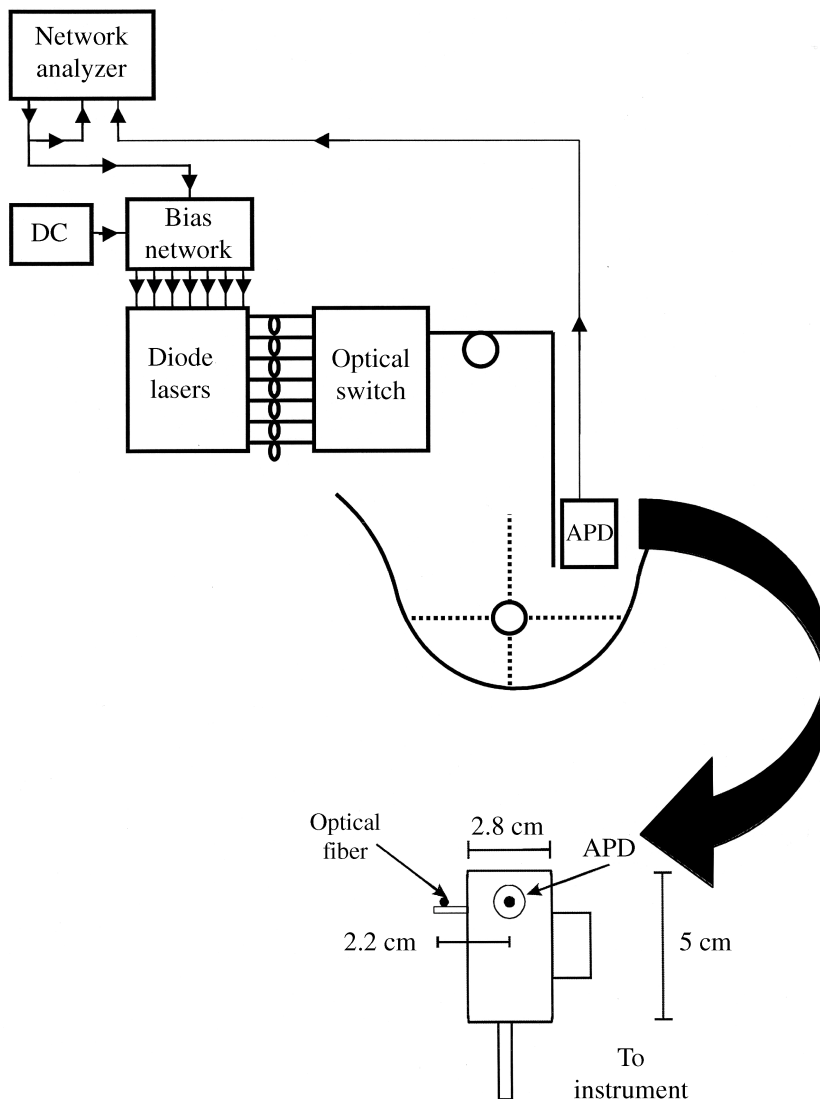
Figure 1. Schematic drawing of FDPM instrument, hand-held probe, and measurement map. The components of the instrument are the diode lasers, avalanche photodiode (APD), network analyzer, steady-state current source (DC), bias network, and optical switch. Measurements were performed with a hand-held probe (close-up at bottom of Figure) that contained the APD and a source optical fiber. The measurement location was in the center of the left upper outer quadrant of the breast, as indicated.

onds per wavelength, with a 2-second delay between each laser diode in the system because of switching considerations. The system was wheeled into a medical clinic for each measurement. Instrumental artifacts were removed by means of calibration on a tissue-simulating phantom with known absorption and scattering properties.

Measured Parameters and Data Analysis

The amplitude and phase of a NIR diffusive light wave demodulates and retards, respectively, as the wave propagates through multiple-scattering media such as tissue. The real and imaginary parts of this diffuse wave were fit simultaneously to a light-diffusion model (the P_1 approximation to the Boltzmann transport equation) (22,23) by minimizing the χ^2 surface with a Marquardt-Levenberg algorithm. This fit determined the absolute optical absorption coefficient μ_a and the absolute optical reduced scattering coefficient μ_s' at each wavelength. Typical μ_a and μ_s' uncertainties, determined from the χ^2 distribution of the fits, are 3% to 1% of their mean values. Precision

errors in actual tissue measurements were determined by performing multiple network analyzer sweeps and multiple probe placements on a given location and were found to be less than 10% for μ_a and 5% for μ_s'.

When the optical properties μ_s' and μ_a are recovered for the seven wavelengths, the spectral dependence of the absorption may be combined with known values of molecular extinction coefficients to calculate physiologically relevant parameters. We assume that bulk breast tissue is composed principally of four NIR absorbers: Hb-R, Hb-O_2, H_2O, and lipids. The concentrations of these absorbers (c) were quantified by solving the equation $\vec{\mu}_a = E\vec{c}$, where E is a 7 × 4 matrix that contains the molar extinction coefficients of the four chromophores at the seven source wavelengths (24–26).

For each measurement, we report four hemoglobin parameters: [Hb-R], [Hb-O_2], the total hemoglobin concentration (THC = [Hb-R] + [Hb-O_2]), and the tissue hemoglobin saturation (S_tO_2 = [Hb-O_2]/THC × 100%), where the characters in square brackets denote concentration in moles per liter. Values for water and lipid content are reported as percentages. The water percentage is the concentration of measured tissue water divided by the concentration of pure water (55.6 mol/L). The lipid percentage indicates the kilograms per liter of lipid measured relative to an assumed "pure" lipid density of 0.9 kg/L. Thus, the water and lipid percentages we report are relative figures of merit compared with pure solutions of the substance and are not strict volume or mass fractions.

The scattering properties of the tissue also yield important physiologic information. NIR scattering in tissue has the following dependence: $\mu_s' = A\lambda^{-SP}$, where A is a constant, λ is the wavelength (in nanometers), and SP is the scatter power. Scatter power is related to the scattering center size (d) compared with the optical wavelength. As an example, scatter power is 4 in the case of Rayleigh scattering ($d \ll \lambda$) and is approximately 1 for large Mie-like scatterers ($d \sim \lambda$).

RESULTS

Sensitivity: Pre- versus Postmenopausal Subjects

Both Figures 2 and 3 present a typical series of measurements of seven absorption and scattering coefficients, respectively. The points represent an average of several measurements in the center of the left upper outer breast quadrants in two subjects, a 32-year-old premenopausal woman and a 54-year-old postmenopausal woman. Error bars indicate the SDs of repeated measurements. There are vast absorption and scattering differences between
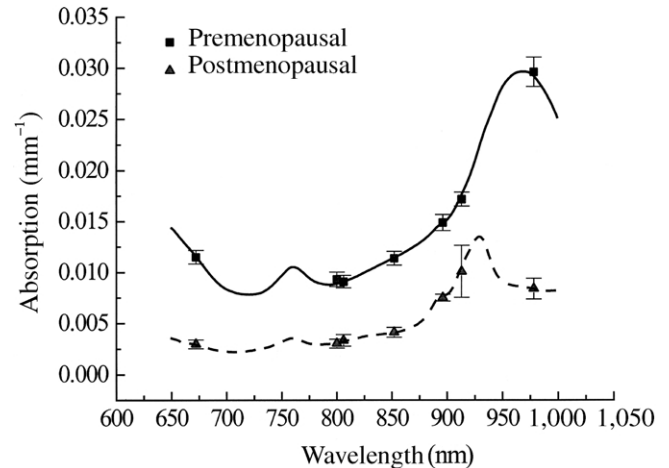

Figure 2. Measured absorption spectra for a 32-year-old premenopausal subject (■, solid line) and a 54-year-old postmenopausal subject (▲, dashed line). Points represent the average of several measurements, and lines represent a least-squares fit (extrapolated to all wavelengths) based on the assumption that breast absorption is due only to Hb-R, Hb-O_2, H_2O, and lipids. Error bars show the SDs of repeated measurements. Concentrations of chromophores from this measurement are listed in Table 1.
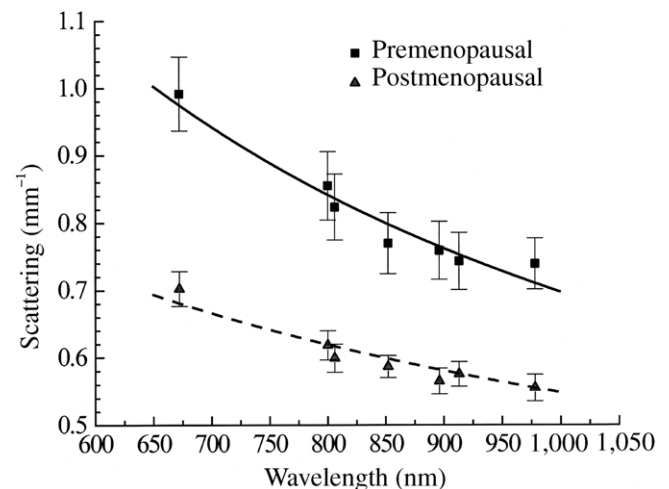

Figure 3. Measured scattering spectra for the same subjects as in Figure 2. The lines represent a fit to $\mu_s' = A\lambda^{-SP}$, where μ_s' is the reduced scattering coefficient (per millimeter), A is a constant, λ is the wavelength (in nanometers) and SP is the scatter power. Results of the fit from this measurement are listed in Table 1. Error bars show the SDs of repeated measurements.

pre- and postmenopausal breast tissue. The solid lines in Figure 2 represent a weighted least-squares fit of the seven absorption coefficients, with published extinction coefficients used for Hb-R, Hb-O_2, H_2O, and lipids (24–26). Lines between the measured points have been interpolated. The solid lines of Figure 3 represent a fit of the scattering coefficients to the equation $\mu_s' = A\lambda^{-SP}$.

Table 1
Measured Physiologic Properties in Breasts of a Premenopausal and a Postmenopausal Subject

Subject	[Hb-R] (μmol/L)	[Hb-O$_2$] (μmol/L)	S$_t$O$_2$ (%)	THC (μmol/L)	[H$_2$O]* (%)	Lipid[†] (%)	Scatter Power
Premenopausal	12.6 ± 0.7	27.9 ± 2.7	68.9 ± 1.3	40.4 ± 2.7	45.1 ± 3.6	29.8 ± 5.6	0.864 ± 0.068
Postmenopausal	2.4 ± 0.5	12.2 ± 1.6	83.7 ± 2.5	14.4 ± 1.9	10.3 ± 0.8	67.5 ± 3.7	0.555 ± 0.036

Note.—Measurements are given as individual means ± SDs for the two subjects represented in Figures 2 and 3.
* Measured concentration relative to pure water.
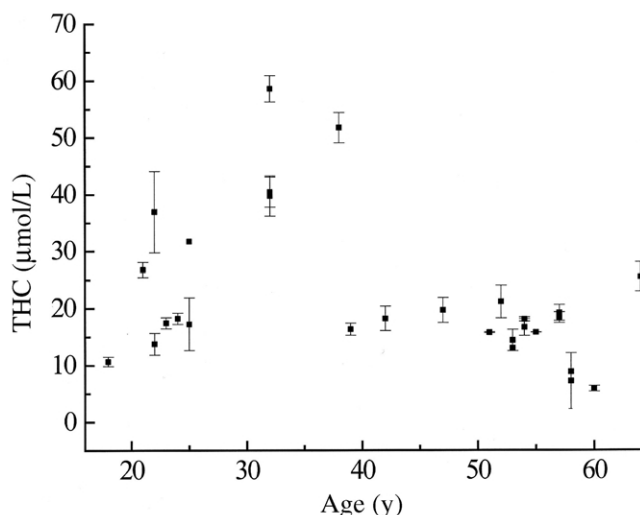[†] Measured mass density relative to pure lipid.

Figure 4. Plot of the THC versus subject age. Premenopausal subjects (<50 years, $n = 15$) show considerable variation with age because of intersubject variations, such as menstrual cycle variations and differences in overall hormone production. Postmenopausal subjects (>50 years, $n = 13$) appear to show a decrease in THC. Error bars show the SDs of repeated measurements.

These optical spectra provide insight into breast tissue composition. There are higher concentrations of hemoglobin (ie, both Hb-R and Hb-O$_2$) in the premenopausal subject, as evidenced by the overall higher absorption in the 670–850-nm range. There is also more water relative to lipids in the premenopausal subject, as revealed by the large water absorption peak at 980 nm. Recovery of the absorption spectra allows calculations of the tissue concentrations of Hb-R, Hb-O$_2$, H$_2$O, and lipids. In addition, the light scattering intensity is substantially lower in the postmenopausal breast. Table 1 summarizes the fitted physiologic properties for the two subjects represented in Figures 2 and 3.

Quantities versus Age

The next three figures present FDPM-measured quantities as a function of subject age. Figure 4 shows the THC, Figure 5 shows the tissue water percentage (referenced to the concentration of pure water), and Figure 6 shows the scatter power. Premenopausal subjects (ie, aged younger than 50 years) display a variety of values in all three plots. This spread is the result of intersubject variations, including, but not limited to, menstrual cycle differences and gynecologic age. The THC, and to a lesser extent the water, seemed to increase in premenopausal subjects (aged 18–39 years), perhaps reaching a peak value near age 30 years. Between the ages of 40 and 49 years, the THC appears to level off, while water and scatter power seem to decline. After age 50 years (predominantly postmenopausal subjects), there is a general decrease with age in THC, water, and scatter power

The late decrease in THC and water correlates well with previous histologic studies showing both atrophy in well-vascularized lobular tissue and an increase in the fat-to-collagen ratio after menopause (15). This decrease is consistent with compositional analysis data showing lower blood and water content for fat versus glandular tissue (27). Scatter power also declines with age after age 50 years. Compared with fat, collagen and glandular tissue scatter light with a higher intensity and a steeper spectral dependence (28). Thus, smaller scatter powers are expected in fatty tissue. Exact knowledge of the weighted biologic contributions to optical tissue scattering is a matter of debate.

Correlation between Absorption and Scattering Information

Figure 7 displays a correlation plot of the measured water and lipid percentages versus scatter power. The lipid percentage is the mass density of lipids in the tissue referenced to the mass density of soybean oil. Note that neither the water nor the lipid percentage represents a strict mass or volume fraction for the tissue (ie, not all components are normalized to 100%). Lines represent fits of water (solid line) and lipids (dashed line) as functions of scatter power.
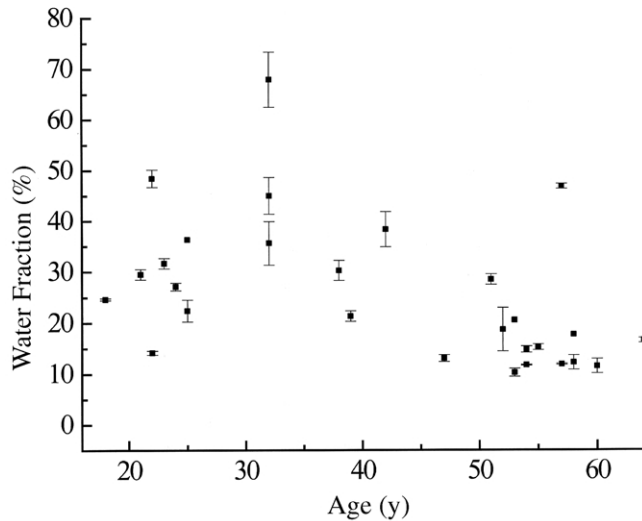
Figure 5. Plot of the measured tissue water percentage versus subject age. Premenopausal subjects show considerable variation over age because of intersubject variations such as menstrual cycle variations and differences in overall hormone production. Postmenopausal and perimenopausal subjects appear to show a decrease in water content. The percentages are water concentrations normalized to the concentration of pure water. Error bars show the SDs of repeated measurements.

Tissue scattering correlates well with the parenchymal composition measured via absorption. As scatter power increases, the lipid percentage decreases ($R^2 = -0.841$, $P < .001$) and the water percentage increases ($R^2 = +0.850$, $P < .001$). The absorption spectra of water and lipids overlap, which can lead to errors in measuring these chromophores. Figure 7, however, clearly shows that both scattering and absorption provide complementary information regarding breast composition, indicating that such errors do not substantially distort our findings.

Tissue Metabolism and Menopause

The S_tO_2 is the percentage fraction of arterial and venous Hb-O_2 that contributes to the tissue THC, and it should not be confused with arterial saturation, which is measured with pulse oximetry. Table 2 presents the measured S_tO_2 in all subjects with a body-mass index less than 40. The average S_tO_2 was approximately 76% for both the premenopausal subjects and those receiving HRT; their means were not significantly different. The S_tO_2 values for the postmenopausal women not receiving HRT, however, were significantly higher, averaging 81.9% $\pm$ 8.8 ($P = .062$).

Decreases in S_tO_2 are associated with increased metabolism (ie, extraction of O_2 from the blood). Tumors, for
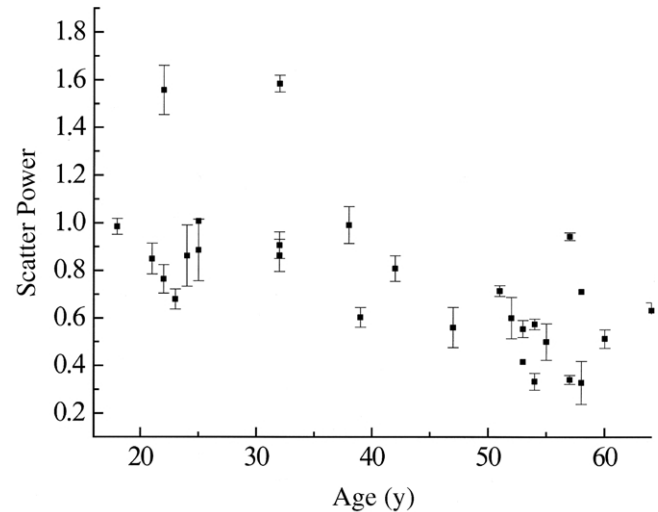

Figure 6. Plot of the measured optical scatter power (in arbitrary units) versus subject age. Optical scatter power refers to the magnitude of the slope of the scattering versus wavelength curve. Premenopausal subjects show considerably higher scatter power than postmenopausal subjects. This general pattern is the same for mammographic density. Error bars show the SDs of repeated measurements.
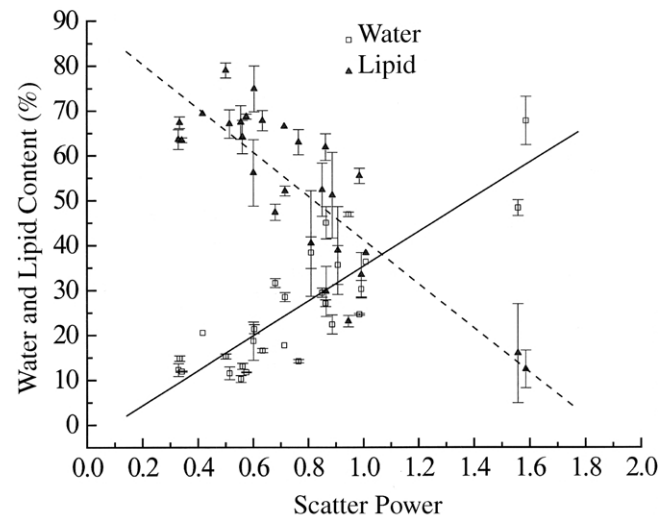

Figure 7. Correlation plots for water percentage (□, solid line) and lipid percentage (▲, dashed line) versus scatter power. Percentages are referenced to the concentration of pure water and the mass density of pure fat. Scatter power correlates with water ($R^2 = +0.850$, $P < .001$) and correlates negatively with lipids ($R^2 = -0.841$, $P < .001$). Error bars show the SDs of repeated measurements.

example, have been shown in vivo to have lower S_tO_2 values than nontumor tissue (6,18,29). The postmenopausal increase in S_tO_2 relative to the premenopausal women and those receiving HRT is plausible, because general tissue metabolism in the breast should decrease

Table 2
Comparison of S_tO_2 Measurements

Subjects	S_tO_2 (%)
Premenopausal ($n = 15$)	76.3 ± 6.4
Receiving HRT ($n = 6$)	76.9 ± 9.2
Postmenopausal ($n = 6$)	81.9 ± 8.8

Note.—Measurements are given as means $\pm$ SDs and are provided for all subjects with a body-mass index of less than 40.

after menopause as the tissue begins to atrophy. The similarity between S_tO_2 values in premenopausal and HRT women suggests that their metabolisms are similar because of the effects of both endogenous and exogenous hormones.

DISCUSSION

Although it is difficult to validate noninvasive in vivo measurements directly, our initial results indicate that the sensitivity of NIR spectroscopy is a reasonable reflection of long-term hormone-controlled breast remodeling. Additional work in the field has demonstrated that short-term menstrual cycle changes are detectable with a similar NIR technique (30). Our results indirectly validate the general accuracy of NIR breast spectroscopy. This quantitative physiologic information is not obtainable with any other noninvasive radiologic method.

An important feature of NIR methods is the ability to characterize quantitatively the breast tissue of women regardless of age, hormonal status, or mammographic density. Increased mammographic density contributes to a 22% false-negative rate and a high false-positive rate (56.2% cumulative risk after 10 examinations) in women less than 50 years of age (31,32). A recent study found that routine initial mammography was not clinically advantageous for women less than 35 years of age (33). Furthermore, the use of HRT in postmenopausal women is known to increase mammographic density (34) and has been recently shown to impede the efficacy of mammographic screening (35,36). The sensitivity of NIR spectroscopy to known biologic processes suggests that optical methods may reveal important new information complementing that provided by conventional diagnostic techniques, particularly in the case of radiographically dense breast tissue.

In general, premenopausal breast tissue is more optically attenuating than postmenopausal breast tissue, in

both absorption and scattering. It is important to note that this trend, particularly in scattering, is also true for mammographic density. Radiographically dense breast tissue is due to differing amounts of fat, collagen, epithelium, and water (37). Although x rays are inherently sensitive to dense electron structures in tissue, such as microcalcifications, NIR photons are naturally sensitive to tissue constituents. Thus, NIR spectroscopy has a unique potential for quantifying the elements of breast tissue that contribute to mammographic density. This observation may be important in screening, since it may identify breast tissue at physiologic risk for malignant transformation, and the technique can be performed easily in all women.

In addition to scattering contrast, we report age-dependent variations in THC, H_2O, and lipids, as well as changes in S_tO_2 for pre- and postmenopausal subjects. Knowledge of the "normal" values of these chromophores will help in evaluating the usefulness of optical methods for detecting and characterizing lesions in the breast. Several investigators have reported a two- to fourfold THC contrast between normal and tumor structures. In vivo tumor S_tO_2 values are also typically lower than those of normal tissue (6,18,29). Thus, detailed studies of normal tissue are essential for determining the sensitivity required of optical instrumentation for detecting lesions in women of varying age and hormonal status. Furthermore, as baseline levels are characterized, data on an individual's absorption and scattering variations could provide important insight into disease appearance and progression. When applied to patients receiving chemotherapy and/or HRT, this information could also be used to generate feedback that would permit customized treatment planning based on individual physiologic response.

REFERENCES

1. Philos Trans R Soc Lond B. 1997; vol 352.
2. Alfano RR, ed. Advances in optical biopsy and optical mammography. Ann NY Acad Sci 1998; vol 838.
3. Heusmann H, Kölzer J, Mitic G. Characterization of female breasts in vivo by time-resolved and spectroscopic measurements in near infrared spectroscopy. J Biomed Opt 1996; 1:425–434.
4. Franceschini MA, Moesta KT, Fantini S, et al. Frequency-domain techniques enhance optical mammography: initial clinical results. Proc Natl Acad Sci U S A 1997; 94:6468–6473.
5. Moesta KT, Fantini S, Jess H, et al. Contrast features of breast cancer in frequency-domain laser scanning mammography. J Biomed Opt 1998; 3:129–136.
6. McBride TO, Pogue BW, Gerety ED, Poplack SB, Osterberg UL, Paulsen KD. Spectroscopic diffuse optical tomography for the quantitative assessment of hemoglobin concentration and oxygen saturation in breast tissue. Appl Opt 1999; 38:5480–5490.
7. Grosenick D, Wabnitz H, Rinneberg HH, Moesta KT, Schlag PM. Development of a time-domain optical mammograph and first in vivo applications. Appl Opt 1999; 38:2927–2943.

8. Colak SB, van der Mark MB, Hooft GW 't, Hoogenraad JH, van der Linden ES, Kuijpers FA. Clinical optical tomography and NIR spectroscopy for breast cancer detection. IEEE J Sel Top Quant 1999; 5:1143–1158.

9. Tromberg BJ, Shah N, Lanning R, et al. Non-invasive in vivo characterization of breast tumors using photon migration spectroscopy. Neoplasia 2000; 2:1–15.

10. Holboke MJ, Tromberg BJ, Li X, et al. Three-dimensional diffuse optical mammography with ultrasound localization in a human subject. J Biomed Opt 2000; 5:237–247.

11. Ntziachristos V, Yodh AG, Schnall M, Chance B. Concurrent MRI and diffuse optical tomography of breast after indocyanine green enhancement. Proc Natl Acad Sci U S A 2000; 97:2767–2772.

12. Suzuki K, Yamashita Y, Ohta K, Kaneko M, Yoshida M, Chance B. Quantitative measurement of optical parameters in normal breasts using time-resolved spectroscopy: in vivo results of 30 Japanese women. J Biomed Opt 1996; 1:330–334.

13. Quaresima V, Matcher SJ, Ferrari M. Identification and quantification of intrinsic optical contrast for near-infrared mammography. Photochem Photobiol 1998; 67:4–14.

14. Cubeddu R, Pifferi A, Taroni P, Torricelli A, Valentini G. Noninvasive absorption and scattering spectroscopy of bulk diffusive media: an application to the optical characterization of human breast. Appl Phys Lett 1999; 74:874–876.

15. Thomsen S, Tatman D. Physiological and pathological factors of human breast disease that can influence optical diagnosis. Ann N Y Acad Sci 1998; 838:171–193.

16. Fishkin JB, Gratton E. Propagation of photon-density waves in strongly scattering media containing an absorbing semi-infinite plane bounded by a straight edge. J Opt Soc Am A Opt Image Sci Vision 1993; 10:127–140.

17. Yodh A, Chance B. Spectroscopy and imaging with diffusing light. Phys Today 1996; 48:34–40.

18. Fishkin JB, Coquoz O, Anderson ER, Brenner M, Tromberg BJ. Frequency-domain photon migration measurements of normal and malignant tissue optical properties in a human subject. Appl Opt 1997; 36:10–20.

19. Cutler M. Transillumination as an aid in the diagnosis of breast lesions. Surg Gynecol Obstet 1929; 48:721–728.

20. Patterson MS, Chance B, Wilson BC. Time resolved reflectance and transmittance for the non-invasive measurement of tissue optical properties. Appl Opt 1989; 28:2331–2336.

21. Pham T, Coquoz O, Fishkin J, Anderson EA, Tromberg BJ. A broad bandwidth frequency domain instrument for quantitative tissue optical spectroscopy. Rev Sci Instrum 2000; 71:1–14.

22. Kaltenbach JM, Kaschke M. Frequency- and time-domain modeling of light transport in random media. In: Müller GJ, Chance B, Alfano RR, et al, eds. Medical optical tomography: functional imaging and monitoring, series IS11. Bellingham, Wash: Society of Photo-Optical Instrumentation Engineers, 1993; 65–86.

23. Fishkin JB, Fantini S, vandeVen MJ, Gratton E. Gigahertz photon density waves in a turbid medium: theory and experiments. Phys Rev E 1996; 53:2307–2319.

24. Wray S, Cope M, Delpy DT, Wyatt JS, Reynolds EO. Characterization of the near infrared absorption spectra of cytochrome aa3 and haemoglobin for the non-invasive monitoring of cerebral oxygenation. Biochim Biophys Acta 1988; 933:184–192.

25. Hale GM, Querry MR. Optical constants of water in the 200-nm to 200-μm wavelength region. Appl Opt 1973; 12:555–563.

26. Eker C. Optical characterization of tissue for medical diagnostics. Lund, Sweden: Lund Institute of Technology, 1999.

27. Duck FA. Physical properties of tissue. London, England: Academic Press, 1990; 320–328.

28. Peters VG, Wyman DR, Patterson MS, Frank GL. Optical properties of normal and diseased human breast tissues in the visible and near infrared. Phys Med Biol 1990; 35:1317–1334.

29. Fantini S, Walker SA, Franceschini MA, Kaschke M, Schlag PM, Moesta KT. Assessment of the size, position, and optical properties of breast tumors in vivo by noninvasive optical methods. Appl Opt 1998; 37:1982–1989.

30. Cubeddu R, D'Andrea C, Pifferi A, Taroni P, Torricelli A, Valentini G. Effects of the menstrual cycle on the red and near-infrared optical properties of the human breast. Photochem Photobiol 2000; 72:383–391.

31. Kerlikowske K, Barclay J. Outcomes of modern screening mammography. J Natl Cancer Inst Monogr 1997; 169:105–111.

32. Elmore JG, Barton MB, Moceri VM, Polk S, Arena PJ, Fletcher SW. Ten-year risk of false positive screening mammograms and clinical breast examinations. N Engl J Med 1998; 338:1089–1096.

33. Hindle WH, Davis L, Wright D. Clinical value of mammography for symptomatic women 35 years of age and younger. Am J Obstet Gynecol 1999; 180:1484–1490.

34. Baines CJ, Dayan R. A tangled web: factors likely to affect the efficacy of screening mammography. J Natl Cancer Inst 1999; 91:833–838.

35. Laya MB, Larson EB, Taplin SH, White E. Effect of estrogen replacement therapy on the specificity and sensitivity of screening mammography. J Natl Cancer Inst 1996; 88:643–649.

36. Litherland JC, Stallard S, Hole D, Cordiner C. The effect of hormone replacement therapy on the sensitivity of screening mammograms. Clin Radiol 1999; 54:285–288.

37. Oza AM, Boyd NF. Mammographic parenchymal patterns: a marker of breast cancer risk. Epidemiol Rev 1993; 15:196–208.